The Canadian Mineralogist
Vol. 44, pp. 775-794 (2006)

STRUCTURAL ENVIRONMENT OF Nb^{5+} IN DRY AND FLUID-RICH (H_2O, F) SILICATE GLASSES: A COMBINED XANES AND EXAFS STUDY

PAULA C. PIILONEN[§]

Research Division, Canadian Museum of Nature, P.O. Box 3443, Station D, Ottawa, Ontario K1P 6P4, Canada

FRANÇOIS FARGES

Laboratoire de Minéralogie (USM 201), Muséum National d'Histoire Naturelle, CNRS UMR 7160, 61, rue Buffon, F-75005 Paris, France and Department of Geological and Environmental Sciences, Stanford University, Stanford, California 94305-2115, USA

ROBERT L. LINNEN

Department of Earth Sciences, University of Waterloo, Waterloo, Ontario N2L 3G1, Canada

GORDON E. BROWN JR.

Department of Geological and Environmental Sciences, Stanford University, Stanford, California 94305-2115, USA and Stanford Synchrotron Radiation Laboratory, Menlo Park, California 94025, USA

MARCIN PAWLAK AND ALLEN PRATT

CANMET, Mining and Mineral Sciences Laboratory, Natural Resources Canada, Ottawa, Ontario K1A 0G1, Canada

ABSTRACT

We performed Nb *K*-edge XAFS spectroscopy experiments on a series of model compounds, natural glasses and anhydrous and fluid-bearing (H_2O, F) synthetic glasses doped with 0.1 to 5 wt.% Nb_2O_5. In addition, we decribe a new ICP–AES method to provide chemical information on micro quantities of glass samples. In dry, H_2O- and F-bearing peraluminous and peralkaline glasses, Nb^{5+} is present as NbO_6 moeties. These share corners with SiO_4 and AlO_4 tetrahedra through non-bridging oxygen (NBO) atoms. No evidence for 4-, 5- or 7-coordinated Nb was found. Slight changes in site centrosymmetry were detected among the compositions (ordered in NBO-rich compositions, more disordered and distorted in peraluminous ones). In agreement with Nb_2O_5 solubility experiments, bond-valence theory suggests that network-modifying cations such as Na are present in the vicinity of Nb. This environment most closely resembles those observed in alkali niobosilicates such as vuonnemite and labuntsovite-group minerals. In dry, peraluminous glasses, the sites containing Nb are disordered, as in columbite. Similar information on speciation was obtained for a set of natural glasses. The local environment around the Nb atoms is therefore highly sensitive to melt depolymerization, alkalinity and H_2O, F contents, all of which will increase the solubility of Nb in the melt and explains a number of its geochemical properties in evolved magmatic systems.

Keywords: niobium, X-ray absorption spectroscopy, synthetic glasses, octahedral coordination, solubility.

SOMMAIRE

Une série de minéraux et de verres naturels et synthétiques (0.1–5 wt.% Nb_2O_5, dopés en H_2O, en fluor, ou les deux) ont été étudiés par spectroscopie XAFS au seuil *K* de Nb. Également, une nouvelle méthode ICP–AES est présentée qui permet d'analyser des micro-quantités d'échantillons dilués en Nb. Dans tous les verres, des unités $Nb^{5+}O_6$ sont détéctées qui partagent des sommets avec des tétraèdres SiO_4/AlO_4 via des atomes d'oxygène non-pontants (ONP). Aucun Nb en coordinence 4, 5 ou 7 n'a été détecté. De légères variations dans la centrosymmétrie des sites ont été mesurées (ordonnée et distordue, pour, respectivement, des compositions riches en ONP et peralumineuses). La théorie des forces de liaison suggère que les cations modificateurs de réseau (comme Na) sont présents autour de Nb. En accord avec les données sur la solubilité de Nb_2O_5, ces environnements

§ *E-mail address*: ppiilonen@mus-nature.ca

sont proches de ceux rencontrés dans des niobiosilicates alcalins tels la vuonnemite ou les minéraux du groupe de la labuntsovite. Dans les verres anhydres et peralumineux, les sites du Nb sont distordus comme dans la columbite. Ces informations de spéciation ont aussi été observées pour trois verres naturels. Ainsi, l'environnement local du Nb est fortement sensible à la dépolymérisation du magma, son alcalinité et ses teneurs en H_2O et F, qui augmentent la solubilité du Nb et expliquent un certain nombre de ses propriétés géochimiques dans les magmas tardifs.

Mots-clés: niobium, spectroscopie de l'absorption des rayons X, verres synthétiques, coordinence octaédrique, solubilité.

Introduction

The pentavalent high-field-strength cation Nb is highly incompatible in most natural igneous systems (*cf.* Möller 1986, Černý & Ercit 1989, Neiva 1999). As a trace element, it is thus an important petrogenetic indicator, providing evidence on the magmatic and hydrothermal conditions under which it was fractionated (Pollard 1989a, b). A growing body of evidence suggests that the behavior of Nb is highly dependent on the alkalinity, SiO_2 activity, and volatile-phase composition of the parental melt or fluid.

Niobium is a highly incompatible element in SiO_2-undersaturated peralkaline systems and shows a high solubility until the final stages of crystallization, at which time it forms alkali niobosilicates, Nb carbonates and Nb oxides (Dunn & McCallum 1982, Černý & Ercit 1989, Keppler 1993, Linnen & Keppler 1997, Horng *et al.* 1999). Furthermore, Nb is also highly mobile in F-rich alkaline systems, and can be leached from earlier-formed minerals by hydrothermal fluids, becoming concentrated, and subsequently precipitated, in veins and fractures (Möller 1986). In particular, Nb is known to be highly mobile in fenitizing fluids enriched in Na, F and Fe^{3+} (Möller 1986). This is in striking contrast to its behavior in SiO_2-saturated metaluminous or peraluminous systems, where Nb is concentrated into Ti phases such as rutile, ilmenite and titanite, and does not form discrete Nb minerals, except in the case of extreme Nb enrichment in late-stage granitic pegmatites (*e.g.*, columbite-group minerals). Although ferrocolumbite and manganocolumbite are common in granitic pegmatites, they are rare in peralkaline syenite pegmatites owing to their high solubility in alkaline melts, even at low temperature (Linnen & Keppler 1997).

Recent experimental studies involving Nb have focused on solubility, diffusivity and mobilization in both hydrous and anhydrous systems. In order to understand the behavior of Nb in magmatic systems, we must first characterize the speciation and local environment around Nb in melts. However, Nb is particularly insensitive to most types of spectroscopy, with the exception of Raman scattering, infrared (IR) and X-ray-absorption fine structure (XAFS). Raman scattering studies have shown that Nb forms NbO_6 moeties in silicate glasses (El Jazouli *et al.* 1988, Fukumi & Sakka 1988, 1989, Ellison & Hess 1989, Gao *et al.* 1989, Vogel *et al.* 1989, Cardinal *et al.* 1996, 1997), in agreement with IR (Samuneva *et al.* 1991) and XAFS experiments (Gao *et al.* 1989, Cardinal *et al.* 1997). In contrast, Paris *et al.* (2000) reported other XAFS experiments in which they concluded that Nb coordination in a variety of dry glasses ranges between 4 and 7. In this study, we utilize the unique ability of XAFS spectroscopy (XANES and EXAFS) to elucidate the local structure and coordination geochemistry of Nb in silicate melts. In addition, a novel method of ICP–AES analyses of micro-quantities of material has been developed and is presented.

We present data for sodium disilicate (NS2), sodium trisilicate (NS3), and a series of dry, H_2O-saturated and F-bearing haplogranitic glasses [alumina saturation index (ASI) = molar Al/(Na + K) ratio between 0.6 and 1.2] containing between 0.1 and 5 wt.% Nb_2O_5. These glasses represent compositionally simplified, structural analogues of more complex natural melts. The information obtained from synthetic Nb-bearing glasses can be compared to naturally occurring Nb minerals and volcanic glasses in order to better understand the behavior of Nb in natural systems.

Experimental Methods

Model compounds

Model compounds from a range of granitic and alkaline igneous rocks were chosen to examine Nb in a wide range of crystal-chemical environments. All model compounds contain Nb^{5+} in 6-fold coordination (E_0 in the range 18984 to 18988 eV), with O as the dominant ligand. Included in the model compounds are the Nb silicates vuonnemite (isolated NbO_6: Ercit *et al.* 1998) and labuntsovite (chains of corner-shared NbO_6: Chukanov *et al.* 1999), the orthophosphate olmsteadite (isolated NbO_6: Moore *et al.* 1976), and two Nb oxides, pyrochlore (3D framework of NbO_6) and columbite (chains of edge-sharing NbO_6: Santos *et al.* 2000). Structural details and chemical formulae for each of the model compounds can be found in Table 1.

Nb glass synthesis

The Nb-bearing glasses (0.1 to 5 wt.% Nb_2O_5) were quenched from melts at 800°C and 2 kbar. Two haplogranitic compositions were investigated: (1) peralkaline (ASI 0.6) and (2) peraluminous (ASI 1.2). The ASI series of glasses was synthesized by R.L. Linnen at the Bayerisches Geoinstitut, Germany and the University of Waterloo, Canada; they were synthesized such that

the metaluminous composition (ASI 1.0) corresponds to the H_2O-saturated 200 MPa granite minimum, and the peralkaline and peraluminous compositions have the same mol.% SiO_2 and Na:K ratio as the metaluminous composition, with only the ASI ratio being different (*cf.* Linnen & Keppler 1997). Niobium was added to the glasses as reagent-grade Nb_2O_5, mechanically mixed using a mortar and pestle, then homogenized in a cold-seal pressure vessel at 800°C and 200 MPa. "Wet" glasses are close to H_2O-saturated and contain approximately 5 to 6 wt.% H_2O. A number of fluorine-bearing glasses were also synthesized by adding aluminum in the form AlF_3, in addition to Al_2O_3, such that the resulting ASI ratio, SiO_2 content, *etc.*, was the same as the F-free glass. Dry glasses were melted at 1200°C at 1 atmosphere, quenched and ground to a powder. This cycle was then repeated to ensure homogeneity. The intended F content was 4%; approximately half of the F was lost as a volatile during glass synthesis, however. Glasses containing 1000 and 5000 ppm Nb_2O_5 were synthesized by mixing the appropriate proportions of Nb_2O_5-free (dry) and 10,000 ppm Nb_2O_5 glasses. The glasses were then mixed, placed in gold capsules with H_2O, welded shut and homogenized in a cold-seal pressure vessel at 800°C and 200 MPa. A similar procedure was used to produce glasses with 100 and 500 ppm Nb_2O_5, except that the initial glasses were Nb_2O_5-free (dry) and 1,000 ppm Nb_2O_5 glasses.

Additional anhydrous sodium silicate glasses (NS2: $Na_2Si_2O_5$, NS3: $Na_2Si_3O_7$) containing between 1000 ppm Nb and 3 wt.% Nb_2O_5 were synthesized using high-purity SiO_2, Al_2O_3, Na_2CO_3 and Nb_2O_5 powders. The powders were placed into platinum crucibles and heated to 500°C for 12 hours to ensure complete decarbonation. The decarbonated powders were then melted at 1200°C and 1 bar for three to five hours, after which they were rapidly quenched in a cold water bath.

Collection of the XAFS data

Niobium XAFS spectra (both XANES and EXAFS regions) of the model compounds and Nb-bearing silicate glasses were collected at the Stanford Synchrotron Radiation Laboratory (SSRL) on wiggler beam stations 4–1 and 11–2. Room-temperature XAFS spectra were collected at the Nb *K* absorption edge (~19 keV) using a Si(220) double-crystal monochromator and a Stern–Heald fluorescence detector filled with Xe. A 3-mm Zr filter and Ag Soller slits were used to minimize unwanted elastic scattering and filter fluorescence, respectively. The energy resolution of the detector is ~5 eV, mostly due to core-hole-lifetime effects (Kostrun *et al.* 1971). The reproducibility of the energy steps of the monochromator is 0.1 eV. To remove the high-energy harmonics from the incident X-ray beam, the monochromator was detuned, and the energy of the incoming beam reduced by 25%. A Nb foil was used to provide an internal calibration of energy. As the Nb content of many of the glasses is low, five to 10 spectra were averaged together to increase the signal-to-noise ratio. Spectra were collected in fluorescence mode with the fluorescence yield measured as a function of the X-ray energy. The mount containing the powdered sample was placed at an angle of 45° to the incident beam, with the detector at 90° to the incident beam.

TABLE 1. STRUCTURAL INFORMATION ABOUT THE Nb MODEL COMPOUNDS

Mineral	Ideal formula	Structural type	CN	Nb–O range (Å)	Δ	E_0 (eV)
Vuonnemite Mont Saint-Hilaire, Quebec	$Na_{11}TiNb_2(Si_2O_7)_2(PO_4)_2O_3(F,OH)$	isolated NbO_6	6	1.758 – 2.238	50.002	18988.8
Labuntsovite-group mineral, Khibina, Kola Peninsula, Russia	$(K,Ba,Na)(Ti,Nb)(Si,Al)_2(O,OH)_7 \cdot H_2O$	chains of corner-shared $(Ti,Nb)O_6$	6	1.9462 – 1.9884	0.849 – 0.892	19987.3
Olmsteadite Big Chief pegmatite, South Dakota	$KFe^{2+}{}_2(Nb,Ta)(PO_4)_2O_2 \cdot 2H_2O$	isolated NbO_6	6	1.832 – 2.137	31.311	18987.9
Manganocolumbite Africa (exact locality unknown)	$(Mn,Fe)(Nb,Ta)_2O_6$	chains of edge-shared NbO_6	6	1.800 – 2.260	23.391 – 51.335	18986.2
Pyrochlore Oka carbonatite, Quebec	$(Ca,Na)_2Nb_2(OH,F)$	3D framework	6	1.9438	0.000	18984.2

CN: coordination number, Δ: quadratic elongation of polyhedra = $\Sigma[(l_i - l_m) / l_m]^2 / CN] \cdot 10^4$, where l_i is the *M*–O bond length, and l_m is the mean <*M*–O> (Robinson *et al.* 1970).

Analysis of the XAFS data

The XAFS spectra were analyzed using the XAFS package (Winterer 1996). The XANES and EXAFS spectra were normalized in absorbance by fitting the spectral region from 18900 to 19100 eV (region before the pre-edge) using a polynomial function and subtracting this from the background. The value of E_0 was determined to be the inflection point of a combination of an error and Gaussian function modeled at the edge jump (~18992 eV) modeled over the range 18900 to 19100 eV. The EXAFS oscillations were normalized using a cubic spline function, and the normalized spectra were recalculated into k space (where k is the photo-electron wave-vector measured with respect to E_0). Special care was taken to remove multi-electronic excitations from the EXAFS baseline (VIPER code, Klementiev 1989), which creates spurious artifacts in the background that can be seen as low frequencies in the Fourier-transform (FT) and that interfere with the Nb–O pair signal. The normalized EXAFS oscillations were k^3-weighted (range: 3 to 13 Å^{-1}) and Fourier-transformed using a Kaiser–Bessel filter (with a τ value of 4) to examine the contributions from next-nearest neighbors (O and Si) around the Nb atoms. The resultant modulus of the FT is a curve similar to a radial-distribution function (RDF) and shows two contributions to the EXAFS spectra: O first-nearest neighbors and Si–Al second-nearest neighbors (network formers). The FT is uncorrected for phase-shifts of the photoelectron wave and contains only those pair correlations involving the central absorber (Nb). As a result, the model compound pyrochlore [$Ca_2Nb_2O_6(OH,F)$] was used to calculate the back-scattering amplitude and phase-shift functions. The k^3-weighted EXAFS oscillations from each model compound were then fitted using one Nb–O and one Nb–Si shell. Fit parameters include the number of oxygen atoms neighboring the Nb (N), the average Nb–O bond length (R), a Debye–Waller factor, a measure of the static and thermal disorder relative to pyrochlore ($\Delta\sigma^2$), and an anharmonic parameter (third cumulant, ΔC_3), a measure of the asymmetry of the Nb–O distance-distribution function, relative to pyrochlore.

Ab initio calculations of the XANES and EXAFS spectra were performed using the FEFF8.28 package (Rehr *et al.* 1992) for a variety of 4-, 5- and 6-coordinated Nb-bearing compounds with O and F as nearest-neighbor ligands. Spectra were calculated for each of the model compounds, as well as for compounds in which Nb displays a different coordination environment and geometry not yet observed in natural compounds (*i.e.,* 5-coordinated Nb–O and Nb–F geometries). These theoretical spectra were used to help identify key features, in particular those in the pre-edge region, within the XANES spectra for the synthetic glasses.

ICP–AES

Lithium metaborate ($LiBO_2$) is an efficient fusion agent for silicates and other rock-forming minerals. For analyses of silicates, the decomposition may proceed at 900°C for 15 min and is usually performed in a platinum crucible with a ratio of fusion agent to sample from 5:2 to 7:1. The resulting glasses are easily dissolved, yielding solutions that can be used in instrumental methods such as absorption and emission spectroscopy.

High-grade $LiBO_2$ granules were pulverized to obtain a particle size similar to that of the sample. Owing to the limited quantities of sample, 2 mg samples were fused in Pt crucibles at a 1:25 ratio of sample to fusion agent over a two-minute period at 900°C. The resultant melt was dissolved in a mixture of 6% HNO_3, 5% tartaric acid and 2% H_2O_2. Analysis for Nb, Si, Al, K and Na was done by inductively coupled plasma – atomic emission spectroscopy (ICP–AES), using matrix-matched blanks and calibration standards. During the method-development stage, various certified reference materials (CRM) were used to validate the elements of interest; none had certified values for Nb, however. Consequently, Nb spikes using various quantities of certified stock solution (1000 ppm Nb) were investigated and provided acceptable recoveries. Accuracies for the certified reference materials, along with sample reproducibility (% RSD) varied 1 to 5% for Nb, Si, Al, K and Na. Results from micro-ICP–AES are shown in Table 2. A comparison with expected values is shown in Figure 1.

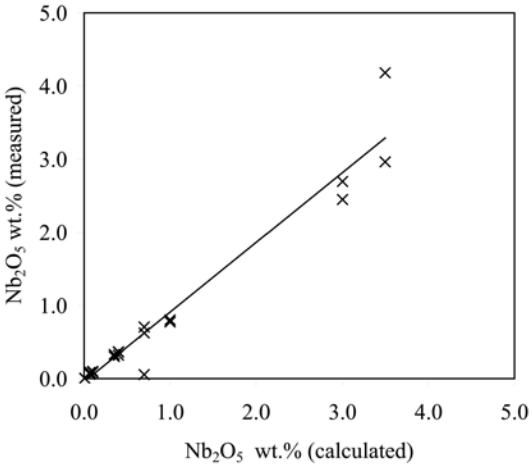

FIG. 1. Calculated versus measured (ICP–AES) Nb_2O_5 (wt.%) for the synthetic glasses. Linear regression: R^2 = 0.953.

TABLE 2. RESULTS FROM MICRO-ICP–AES ANALYSIS OF THE SYNTHETIC GLASSES

Glass	Mass mg	Dilution factor	Nb_2O_5 calc.	Nb_2O_5 meas.	Δ ppm	Δ %	Al ppm	K ppm	Na ppm	Si ppm
STD (OKA-1)	0.1979	5253.21	0.400	0.367	334	8.4	10076	6045	3605	30665
STD (OKA-1)	0.2286	4959.49	0.400	0.362	380	9.5	10006	5952	3528	29011
STD (OKA-1)	0.2203	5208.03	0.400	0.320	802	20.1	9769	6075	3609	28442
NS2, Dry, 1000 ppm Nb	0.20065	5019.17	0.100	0.100	1	0.1	466	388	264072	201748
NS2, Dry, 1 wt.% Nb	0.2127	4482.38	1.000	0.775	2249	22.5	524	287	258366	176363
NS2, Dry, 3 wt.% Nb	0.203	5037.88	3.000	2.448	5520	18.4	302	183	262304	202209
NS3, Dry, 1000 ppm Nb	0.2093	5485.74	0.100	0.087	128	12.8	-127	284	211111	195758
NS3, Dry, 1 wt.% Nb	0.2153	4399.93	1.000	0.802	1977	19.8	396	456	191410	232983
NS3, Dry, 3 wt.% Nb	0.2083	5187.77	3.000	2.696	3044	10.1	335	1283	212374	252033
ASI 0.6, Dry, 1000 ppm Nb	0.1334	8158.17	0.070	0.081	-108	10.8	56433	41386	48713	334410
ASI 0.6, Dry, 2 wt.% F, 1000 ppm Nb	0.203	5409.01	0.070	0.069	10	1.0	61228	43082	50057	375796
ASI 0.6, Wet, 1000 ppm Nb	0.2006	5826.62	0.070	0.072	-22	2.2	57410	42563	47755	343441
ASI 0.6, Dry, 5000 ppm Nb	0.2161	4823.74	0.350	0.331	182	3.6	63834	44308	51898	339133
ASI 0.6, Wet, 5000 ppm Nb	0.2084	5189.54	0.350	0.301	486	9.7	52682	37398	44176	327665
ASI 1.2, Wet, 5000 ppm Nb	0.2091	4722.30	0.350	0.302	471	9.4	79184	27576	32005	373492
ASI 1.2, Wet, 1000 ppm Nb	0.0657	15932.88	0.070	0.060	95	9.5	77832	27803	32403	384650
ASI 1.2, Wet, 100 ppm Nb	0.1957	5512.11	0.007	0.006	13	13.2	76052	29444	33314	357640
ASI 0.6, Dry, 5 wt.% Nb	0.0043	274493.02	3.495	4.181	-6858	13.7	73010	52105	57634	390620
ASI 0.6, Wet, 5 wt.% Nb	0.19705	6506.48	3.495	2.962	5329	10.7	50458	33566	40704	247306
ASI 0.6, Dry, 1 wt.% Nb	0.1897	7006.17	0.699	0.707	-77	0.8	57371	38189	44747	283895
ASI 0.6, Wet, 1 wt.% Nb	0.1789	6616.15	0.699	0.625	739	7.4	52342	34131	40094	349147
ASI 1.2, Wet, 1 wt.% Nb	0.2527	4960.90	0.699	0.055	6441	64.4	6511	2428	2721	30613
ASI 1.2, Dry, 2 wt.% F, 1000 ppm Nb	0.166	7841.57	0.070	0.088	-176	17.6	79009	29303	34141	368065
ASI 1.2, Dry, 1000 ppm Nb	0.175	6554.11	0.070	0.075	-50	5.0	82084	28977	34522	360164
ASI 1.2, Dry, 2 wt.% F, 1000 ppm Nb	0.2522	4937.55	0.070	0.062	78	7.8	49807	35231	40993	345249
ASI 1.2, Wet, 2 wt.% F, 1000 ppm Nb	0.2358	5368.15	0.070	0.059	112	11.2	71198	25521	29813	345910
ASI 1.2, H_2O content unknown, 100 ppm Nb	0.28705	4002.39	0.007	0.007	4	3.6	79818	28004	33075	349638

RESULTS

Model compounds: XANES spectra

Figure 2 shows the Nb *K*-edge XANES spectra for the model compounds in which Nb is in 6-fold coordination. Of note is the presence of a broadened pre-edge feature (I) in all the model compound spectra, suggesting that the environment around Nb deviates from being centrosymmetric. The pre-edge cannot be resolved because of the large core-hole lifetime of the Nb *K*-edge. Octahedrally coordinated d^0 cations such as Nb^{5+}, Ti^{4+}, V^{5+} and Mo^{6+} are usually found in distorted environments, a result of the tendency of the cation toward positional displacement within the octahedron. Distortion increases with increasing formal charge and decreases with increasing size of the cation. Such out-of-center distortions are responsible for many of the optical and electronic properties exhibited by d^0 transition-metal compounds (Samuneva *et al.* 1991, Cohen 1992, Cardinal *et al.* 1996).

Distortions within octahedra occupied by d^0 transition metals may be due to (1) the bonding network (nearest neighbors and bond-valence considerations), (2) lattice stresses (structural compensations), (3) cation–cation repulsion (edge- or face-sharing of polyhedra) and (4) electronic effects (second-order Jahn–Teller distortions; Kunz & Brown 1995). In examining the distortion of an octahedron, both the magnitude and the direction of the distortion must be taken into consideration. Although all four effects will influence the magnitude of the distortion, only the bonding network and cation–cation repulsion will influence the direction of the distortion. Electronic distortions are the result of a second-order Jahn–Teller effect. For such a distortion to occur, the energy gap between the highest occupied (HOMO) and lowest occupied molecular orbits (LUMO) has to be small, a condition dependent on both the charge and size of the cation and the bonding network; the magnitude of the electronic effect is inversely proportional to this energy gap, which will decrease in highly charged, small cations such as V^{5+} and Mo^{6+}. In the case of Nb^{5+} (as well as Ti^{4+} and Ta^{5+}), the influence of electronic effects on the magnitude of the distortion is moderate, and the cation is found in both distorted and undistorted environments, depending

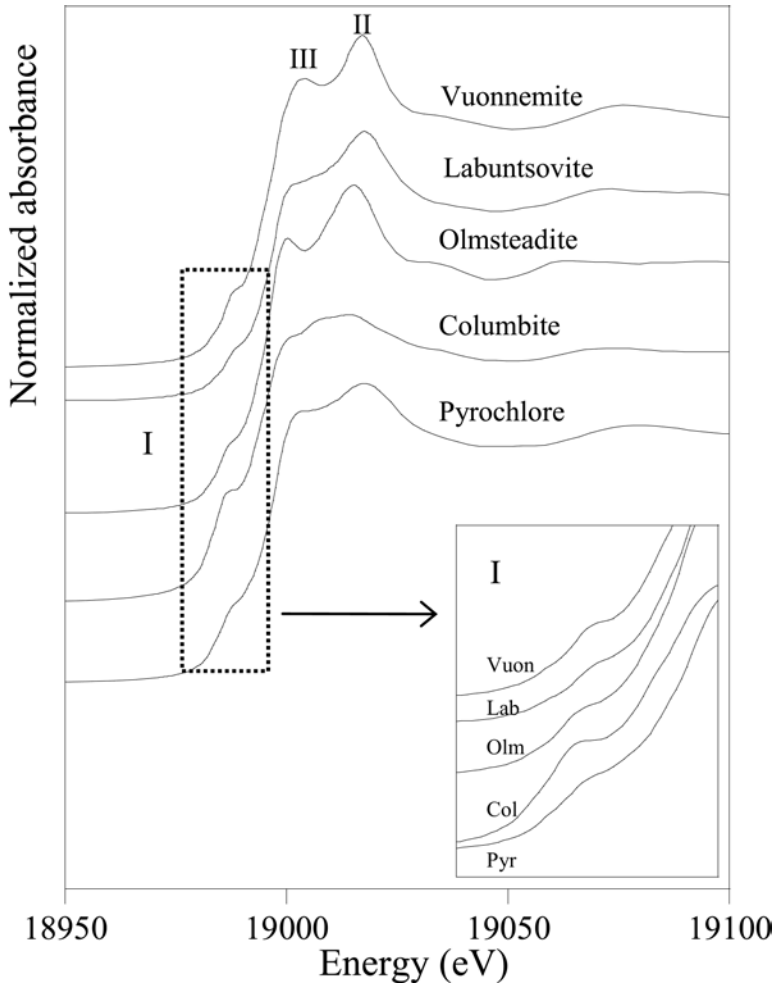

FIG. 2. Nb *K*-edge high-resolution XANES spectra for the model compounds. Nb is 6-coordinated in the model compounds, with Nb–O bond lengths ranging from 1.758 to 2.260 Å. Note the presence of a pre-edge feature (I) in all the model compounds, suggesting that Nb occurs in non-centrosymmetric, distorted sites.

on the structural energy of the crystal and other forces such as structural stresses and cation–cation repulsion (*i.e.*, out-of-center distortions will only occur where structural distortions are present).

In the case of the model compounds used in this study, manganocolumbite has the most intense pre-edge feature, suggesting the largest distortion. The columbite structure consists of edge-sharing NbO_6 octahedra, which increase the degree of cation–cation repulsion compared to structures with corner-shared NbO_6 octahedra; out-of-center distortions are therefore predicted. The remaining model compounds, all of which contain isolated or corner-shared NbO_6, display pre-edge features with similar intensities.

The cubic structure of pyrochlore consists of a 3D network of corner-shared NbO_6 octahedra. Although a long-range, undistorted environment is recognized in single-crystal X-ray-diffraction studies, pyrochlore-group minerals contain a cation site (*A*) that inevitably displays partial occupancy. The presence of vacancies as second-nearest neighbors to Nb atoms in the pyrochlore structure results in local disorder and distortions due to the displacement of O atoms, which are required to accommodate the loss of bond valence from the second-nearest neighbor alkali cations. In addition to structural defects, the pyrochlore from the Niobec mine (Quebec) used in this study is enriched in Th (T.S.Ercit, unpubl. data) and is partially metamict, adding to the

distortion and disordered nature of the local environment around Nb.

In the niobosilicates vuonnemite and labuntsovite, as well as in olmsteadite, NbO_6 octahedra share corners or occur as isolated octahedra; there is no cation–cation repulsion. Owing to bond-valence requirements and structural stresses, the octahedra are elongate, and the cation is displaced within the octahedron toward one of the apices. Megaw (1968a, b) suggested that off-center displacement of small, highly charged [6]-coordinated cations (*e.g.*, Nb^{5+} and Ti^{4+}) occurs where the effective radius of the cation is such that the unstressed *M*–O bond length is less than $1/\sqrt{2}$ times the diameter of the oxygen atom. In these cases, the mutual attraction and repulsion effects within the octahedron result in "stressed" bonds to the point where the anion–anion repulsion has caused the cation–anion bond to be extended beyond its unstressed value. The resultant tension in the O–*M*–O bond length is relaxed by off-center displacement of the cation and relaxation of the O–O edges.

The main edge-crest features (II and III in Fig. 2) are related to single- and multiple-scattering paths of the photoelectron around Nb involving first (II) and second (III) nearest neighbors, respectively, as with Zr (Farges & Rossano 2000). Feature II is directly correlated with the inverse of the square average Nb–O distances (Bianconi *et al*. 1985), whereas feature III is dominantly related to the degree of order around the Nb atom and is more intense in ordered structures. From these edge-crest features, it is evident that a disordered structure is present in the oxides manganocolumbite and pyrochlore, whereas the environment around Nb in the alkali niobosilicates and olmsteadite is more ordered.

FEFF ab initio simulations

Ab initio calculations using the program FEFF were performed for a variety of Nb compounds including those utilized as models, as well as Nb-substituted fresnoite (Ti site) and synthetic Nb–F compounds, to determine the effects of F and varying coordination number on the XANES spectra (Fig. 3). Figures 3A and B depict the calculated XANES spectra for vuonnemite and pyrochlore, model compounds that have NbO_6 octahedra. In the case of vuonnemite, the calculated and experimental spectra are almost identical, including the presence of the pre-edge feature (I). The calculated and experimental spectra for pyrochlore differ in that the

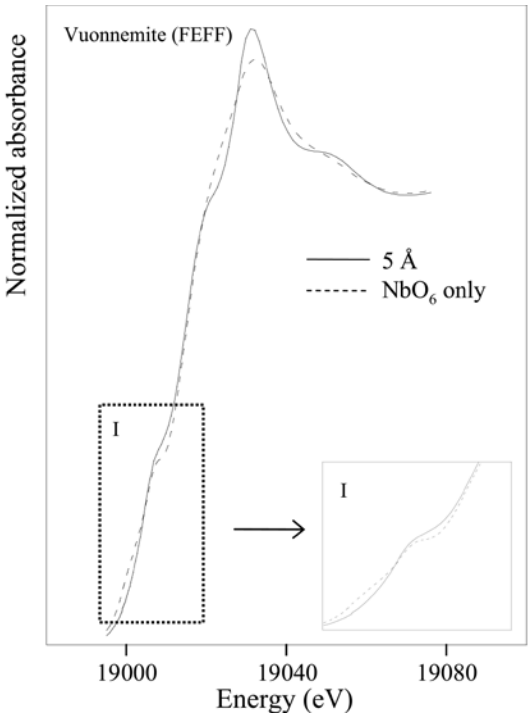

FIG. 3A. *Ab initio* FEFF calculation of the Nb K-edge XANES spectrum for vuonnemite. The solid line represents the calculation for the structure up to 5 Å from the central Nb atom, whereas the dashed line represents the calculated spectrum for the NbO_6 octahedron only. Note the presence of a distinct pre-edge feature (I) in both calculated spectra (insert).

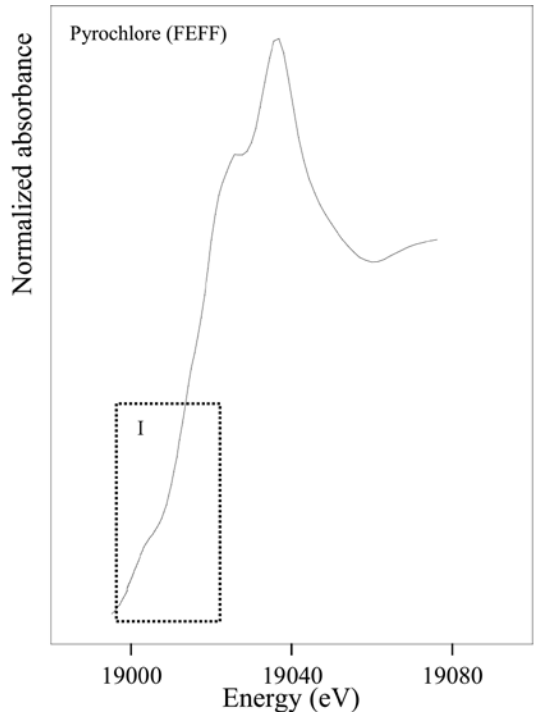

FIG. 3B. *Ab initio* FEFF calculation of the Nb *K*-edge XANES spectrum for pyrochlore.

intensity of feature II in the *ab initio* spectrum is more intense and well defined, because the calculated spectrum does not take into account the defects (vacancies) that are inherent in any natural sample. Figure 3C shows the calculated XANES spectrum for Nb-substituted fresnoite with NbO_5 polyhedra. Of note is the presence of a very distinct and sharp pre-edge feature (I), which is more intense than the weak shoulder observed in the compounds containing NbO_6 octahedra. The strong distinction in the XANES pre-edge features between NbO_5 and NbO_6 polyhedra will allow us to determine the coordination number of Nb in the synthetic glasses. Figure 3D depicts the calculated XANES spectra for three synthetic compounds containing NbF_6 and NbF_7 polyhedra. Of note is the similarity in the pre-edge feature (I) in compounds containing NbO_6 and NbF_6 polyhedra.

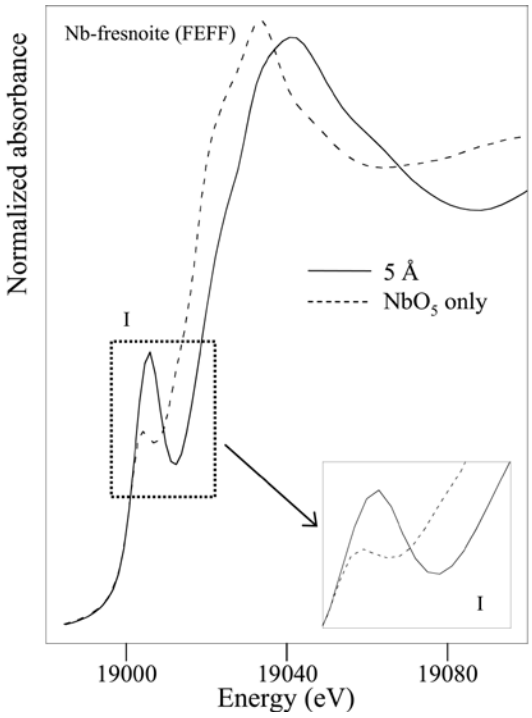

FIG. 3C. *Ab initio* FEFF calculation of the Nb *K*-edge XANES spectrum for Nb-substituted fresnoite with 5-coordinated NbO_5 (Markgraf *et al.* 1985). The solid line represents the calculated spectrum for the structure up to 5 Å from the central Nb atom, whereas the dashed line represents the calculated spectrum for the NbO_5 polyhedron only. Note the presence of a distinct, intense pre-edge feature (I) in both calculated spectra (insert), which is not observed in compounds with NbO_6.

Model compounds: EXAFS spectra

Figure 4A shows the normalized, k^3-weighted EXAFS spectra for the model compounds. The experimental data are shown as a solid line, whereas the best calculated model is shown as a dashed line. The spectra were modeled using a two-shell fit (Nb–O and Nb–*M* (where *M* = Ca, Si, P, Ti, Mn) based on pyrochlore. In Table 3, we list the fit parameters for each of the refinements. The FTs of each of the normalized, k^3-weighted EXAFS spectra are shown in Figure 4B. Two main contributions are detected within each of the model compounds: a Nb–O contribution between 1.95 and 2.03 Å, and a second contribution at 3.45 to 3.56 Å, the result of Nb–Ca, Nb–Si, Nb–Mn, Nb–Ti or Nb–P next-nearest neighbors. The EXAFS data are in agreement with values obtained for the model compounds by single-crystal X-ray-diffraction studies (Table 3).

Nb glasses: XANES spectra

Figure 5 shows the Nb *K*-edge XANES spectra for the synthetic glasses. The spectra most closely

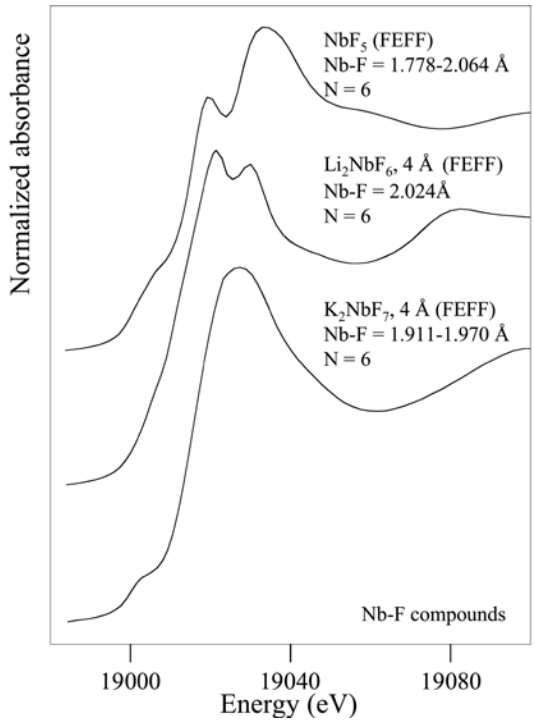

FIG. 3D. *Ab initio* FEFF calculation of the Nb *K*-edge XANES spectrum for various synthetic Nb–F compounds with NbF_6 and NbF_7 polyhedra: NbF_6 (Edwards 1964), Li_2NbF_6 (de Bournonville *et al.* 1986), and K_2NbF_7 (NbF_7 polyhedra, Brown & Walker 1966).

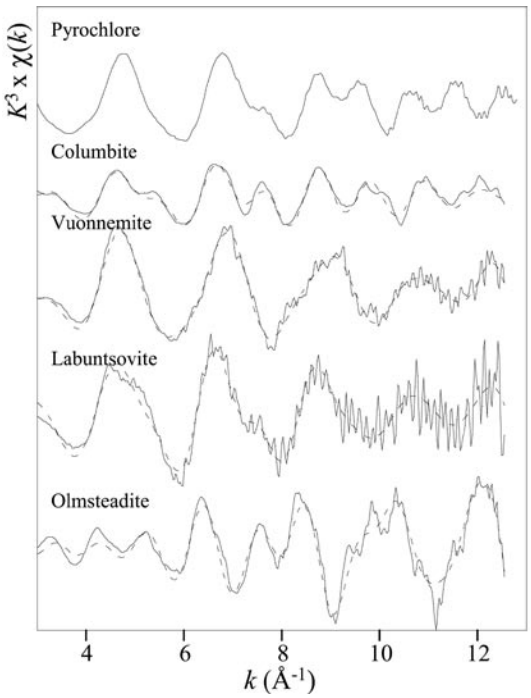

FIG. 4A. Nb *K*-edge normalized (k^3-weighted) EXAFS spectra for the model compounds (solid lines) and the best model (dashed lines) calculated based on pyrochlore (two-shell fit).

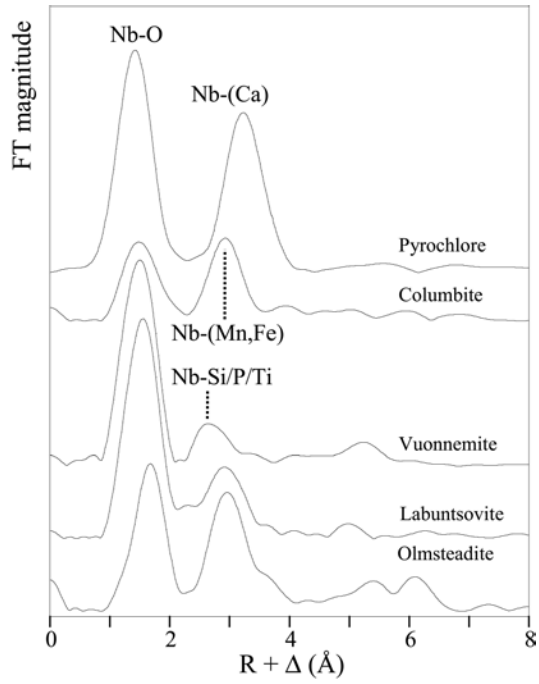

FIG. 4B. Fourier transforms of the normalized (k^3-weighted) EXAFS spectra shown in Figure 4A showing the two contributions around Nb: O first- and (Si, Na, Ca, P, Ti, Mn) second-nearest neighbors.

TABLE 3. EXAFS FIT RESULTS FOR THE MODEL COMPOUNDS, RELATIVE TO PYROCHLORE

Model compounds	Method	E_0 eV	Shell	N	R Å	σ^2 Å^2 × 10^3	ΔE eV	χ^2
mangano-	EXAFS	18986.2	O	5.6	2.03	0.001	0.2	1.3
columbite	XRD		O	6	2.02			
labuntsovite-	EXAFS	18987.3	O	5.2	2.04	0.010	0.2	0.4
group			Si	10.3	3.45	0.09		
mineral	XRD		O	6	1.95			
			Si	4	3.24			
			Ti	2	3.56			
olmsteadite	EXAFS	18987.9	O	6.2	2.02	0.012	-0.1	1.6
			Si	1.9	3.54	0.45		
	XRD		O	6	1.98			
			P	4	3.37			
			Fe	4	3.6			
vuonnemite	EXAFS	18988.8	O	6.1	2.04	0.004	-0.4	1.4
			Si	6	3.46	3.48		
	XRD		O	6	1.96			
			Si+P	4+1	3.46			

Note: N: number of nearest neighbors, R: average distance to central Nb, σ^2: Debye–Waller factor relative to pyrochlore.
Both ΔE and χ^2 are measures of the quality of fit.

resemble those of the alkali niobosilicates (vuonnemite and labuntsovite) and show large discrepancies with the oxide phases manganocolumbite and pyrochlore, suggesting that no saturation in Nb_2O_5 (undissolved or nucleated Nb_2O_5) occurred during synthesis of the glasses.

There is no evidence for 5-coordinated Nb in any the glasses; the intense pre-edge feature observed in the calculated XANES spectrum of Nb-substituted fresnoite, indicative of NbO_5 groups, is not present. Similar conclusions can be drawn about the absence of highly non-centrosymmetric 4- and 7-coordinated sites around Nb, as all glasses studied contain pre-edge features similar to those observed in model compounds with 6-coordinated Nb. A weak pre-edge feature (I) is present in all natural and synthetic glasses, indicating the presence of a site not too far from centrosymmetry. In the NS2 and NS3 glasses (Fig. 5), the feature is less intense than that of the ASI glasses, suggesting that the sites containing Nb are closer to being centrosymmetric and undistorted. In the ASI glasses, the pre-edge feature increases with increasing Nb_2O_5 content, suggesting an increase in distortion of the NbO_6 octahedra (Figs. 5A, B). A comparison of ASI 0.6 and ASI 1.2 at 1000 ppm Nb suggests an increase in the intensity of the pre-edge

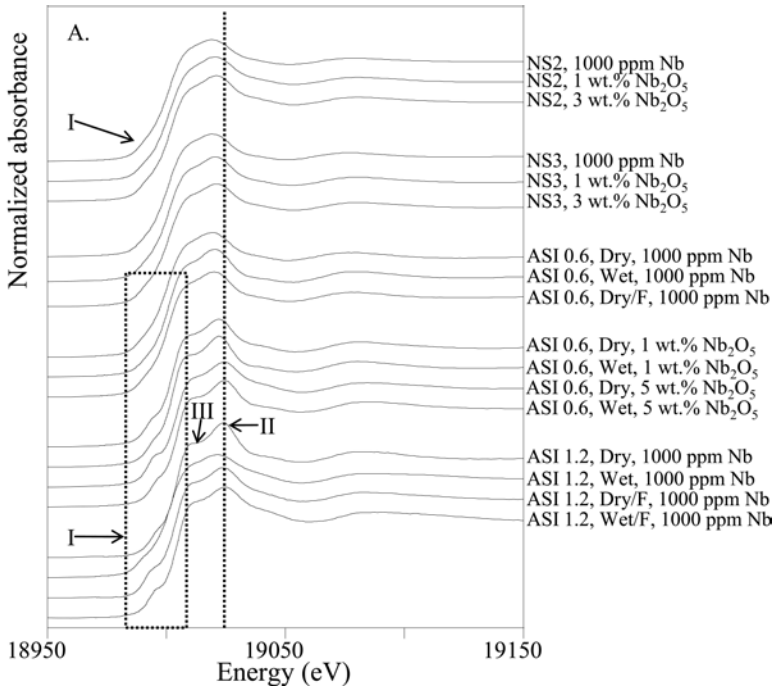

FIG. 5A. Nb *K*-edge high-resolution XANES spectra for synthetic glasses.

with increasing peraluminosity (ASI 1.2), indicating increasing radial distortion and non-centrosymmetry of the environment around Nb in the latter glass. Similarly, within the peraluminous (ASI 1.2) glasses, the presence of both H_2O and F appears to increase the degree of distortion of the local environment around Nb; the pre-edge appears to be insensitive to F in the peralkaline (ASI 0.6) glasses.

All glasses show a doublet in the main edge (II and III in Fig. 5), similar to those for 6-coordinated Zr in synthetic glasses (Farges *et al*. 1991, Farges & Rossano 2000). However, the behavior of the main edge-crest in response to glass composition is of significant interest. In the NS2 and NS3 glasses, the doublet is not well resolved, suggesting a disordered local structure; the edge-crest is not affected by the Nb_2O_5 concentration, consistent with what is observed in the pre-edge. In contrast, the ASI 0.6 and 1.2 glasses show a resolved doublet (II and III in Figs. 5A, C) that varies in intensity depending on the glass composition. In general, NbO_6 groups in the ASI 1.2 (peraluminous) glasses are more ordered than the ASI 0.6 (alkaline) glasses, consistent with the degree of polymerization expected within each of these compositions. Within the ASI 0.6 glasses, the doublet becomes more resolved, and the local structure more ordered, as the Nb_2O_5 content increases. At a constant Nb content of 1000 ppm, distinct differences in the edge-crest features are observed between the ASI 1.2 and 0.6 glasses (Fig. 5C). In the ASI 1.2 suite, the presence of both H_2O and F result in a decrease in a resolution of the doublet features and in decreasing degree of order in the Nb environment Dry > Dry + F > Wet. In general, the H_2O-saturated ASI 1.2 glasses show a more intense pre-edge feature and a wider, less-resolved main edge-feature than dry glasses, indicating a more distorted and less ordered local environment around the Nb atom. This is what is expected as the glass undergoes depolymerization with the addition of both F and H_2O, suggesting that Nb in the peraluminous glasses is directly affected by the increase in non-bridging oxygen atoms (NBO) produced by the breakage of $Si–O_{Br}–Si$ bonds and resultant formation Si–(F,OH) or $^{[4]}$Al–(F,OH) complexes (Dingwell *et al*. 1985, Giordano *et al*. 2004). In contrast, the presence of H_2O and F in the peralkaline ASI 0.6 glasses appear to slightly *increase* the resolution of the doublet, indicating a more ordered NbO_6 environment in the sequence Wet > Dry + F > Dry. This is contrary to what is expected, as both H_2O and F depolymerize (or at least inhibit the formation of) highly polymerized units within the silicate melt network. It is possible that the reversal in behavior observed is a combination of the fact that (1) the peralkaline glass is less polymerized and more disordered to begin with, (2) the concentration of K

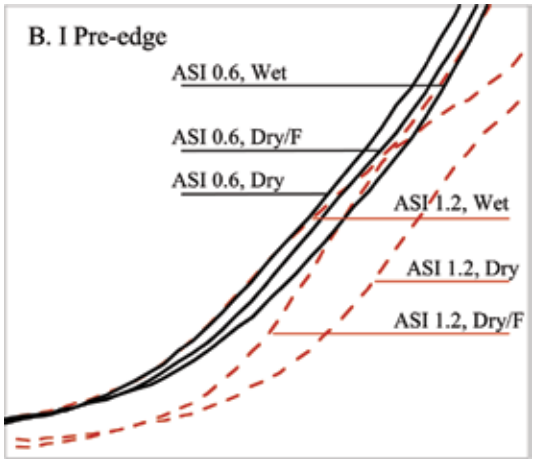

FIG. 5B. Note the increase in intensity of the pre-edge feature (I), indicating increasing distortion of the Nb site with decreasing alkalinity and Nb content in the ASI glasses (ASI 0.6: black, ASI 1.2: red). In NS2 and NS3 (Fig. 5A), the pre-edge is almost non-existent, indicating centrosymmetric (non-distorted) Nb sites. At 1000 ppm, the two sets of glasses display inverse trends with increasing H_2O + F. In the ASI 0.6 (peralkaline) glasses, the NbO_6 octahedra become more ordered and centrosymmetric with increasing H_2O and F, such that Wet + F > Dry + F > Dry. The reverse is observed in the ASI 1.2 (peraluminous) glasses, in which order and centrosymmetry decrease with increased level of H_2O and F, such that Dry > Dry + F > Wet + F.

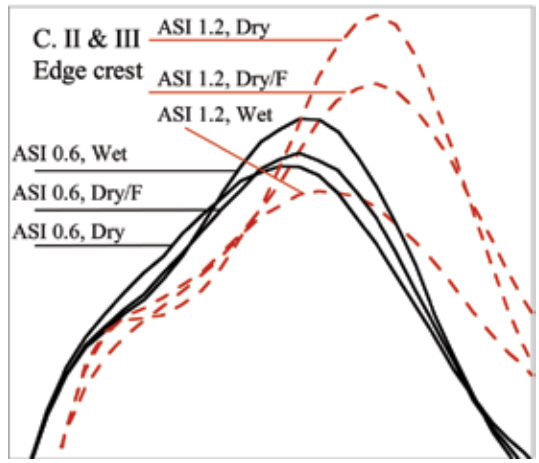

FIG. 5C. Main edge-features (II and III) in ASI glasses. Note the general increased resolution of the doublet with increasing alkalinity. Within the ASI suites, the same reverse trend is noted as observed in the pre-edge (Fig. 5B).

+ Al far exceeds that required to charge-compensate the dominant $^{[4]}Al$ species in the melt, and is therefore available to act as charge-balancers for the Nb^{5+} cations, and (3) the role played by H_2O and F in the peralkaline glasses is different than that in the peraluminous glasses. At concentrations of 1 and 5 wt.%, the pre-edge of H_2O- and F-bearing glasses is less intense, indicating that with increasing Nb_2O_5, the NbO_6 octahedron becomes less distorted.

Natural glasses: XANES spectra

Figure 6 shows the Nb *K*-edge spectra for the natural glasses. The spectra are very similar to those observed for the ASI synthetic glasses, suggesting that such glasses are good analogues for the local environment of Nb in natural systems. The natural glasses have a weak pre-edge feature and a resolved doublet in the main edge-crest; the broad, unresolved doublet observed in the NS2 and NS3 glasses is not present, indicating that the environment around Nb is more ordered, similar to what is observed for the dry ASI 1.2 glasses.

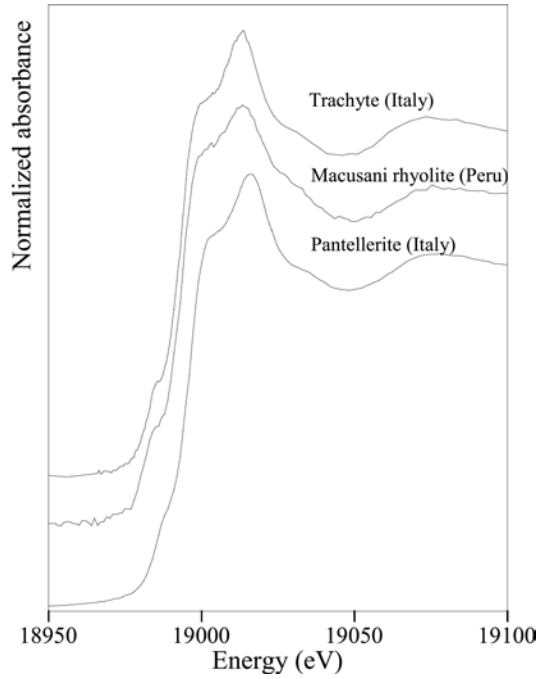

FIG. 6. Nb *K*-edge high-resolution XANES spectra for the natural Nb-bearing volcanic glasses. The natural trachytic and pantelleritic glasses (from the islands of Pantelleria and Stromboli, Italy) have been previously examined in detail by Mahood & Stimac (1990), Pichavant *et al.* (1987) and Farges & Rossano (2000).

Nb glasses: EXAFS spectra

Figure 7A shows the normalized, k^3-weighted EXAFS spectra for the six NS2 and NS3 glasses. The best model for each spectrum is presented (dashed line). All six spectra are similar to each other and closely resemble the spectrum for vuonnemite. Large differences are observed between the NS glasses and the oxide model compounds. The FTs of the normalized k^3-weighted spectra are shown in Figure 7B, and the corresponding fit parameters are listed in Table 4. Two main contributions are detected around the Nb atom: a Nb–O shell with four to seven nearest neighbors and an average bond-length of 2.04 Å ($^{[6]}$Nb–O bond lengths range from 1.74 to 2.54 Å), and a second shell of Nb–Si(Na) with an average bond-length of 3.67 Å.

Figure 8A shows the normalized, k^3-weighted EXAFS spectra for the 1000 ppm ASI glasses (solid line). The best model for each spectrum is presented (dashed line) relative to pyrochlore. The FTs of the normalized k^3-weighted spectra are shown in Figure 8B, and corresponding fit-parameters, in Table 4. As with the NS2 and NS3 glasses, the ASI glasses show two main contributions around the central Nb atoms: a Nb–O shell with 4.5 to 6.6 nearest neighbors and a

TABLE 4. EXAFS FIT RESULTS FOR THE SYNTHETIC GLASSES, RELATIVE TO PYROCHLORE

	E_0 eV	Shell	N	R Å	σ^2 Å$^2 \times 10^3$	ΔE eV	χ^2
NS2, 1000 ppm Nb	19002.0	O	4.1	2.03	8.6	0	0.37
		Si	0.3	3.63	20.8		
NS2, 1 wt.% Nb_2O_5	19002.7	O	6.1	2.04	5.8	2.7	0.99
		Si	1.3	3.7	7.4		
NS2, 3 wt.% Nb_2O_5	19003.0	O	6	2.05	7.7	0	0.77
		Si	6.7	3.53	33.9		
NS3, 1000 ppm Nb	19001.7	O	5.6	2.04	6.8	0	0.51
		Si	–	–	–		
NS3, 1 wt.% Nb_2O_5	19002.4	O	5.5	2.04	0.2	0	0.5
		Si	1.3	3.61	3.2		
NS3, 3 wt.% Nb_2O_5	19002.2	O	6.5	2.02	0	-0.4	
ASI 1.2, wet, 1000 ppm Nb	19002.2	O	4.5	1.88	0	0	0.92
		Si	7	3.61	21.8		
ASI 0.6, wet, 1000 ppm Nb	18998.8	O	5.4	1.97	20.1	0	0.9
		Si	6.6	3.48	24		
ASI 0.6, dry, 1000 ppm Nb	19001.6	O	4	2.05	0.8	0	0.94
		Si	4.7	3.47	26.1		
ASI 0.6, dry/F, 1000 ppm Nb	19000.2	O	5.9	2.02	0	0	1.31
		Si	4.2	3.51	16.1		
SD		O	0.4	0.02	0.2	0.5	
		Si	0.7	0.05	1		

Note: N: number of nearest neighbors, R: average distance to central Nb, σ^2: Debye–Waller factor relative to pyrochlore. Both ΔE and χ^2 are measures of the quality of fit.

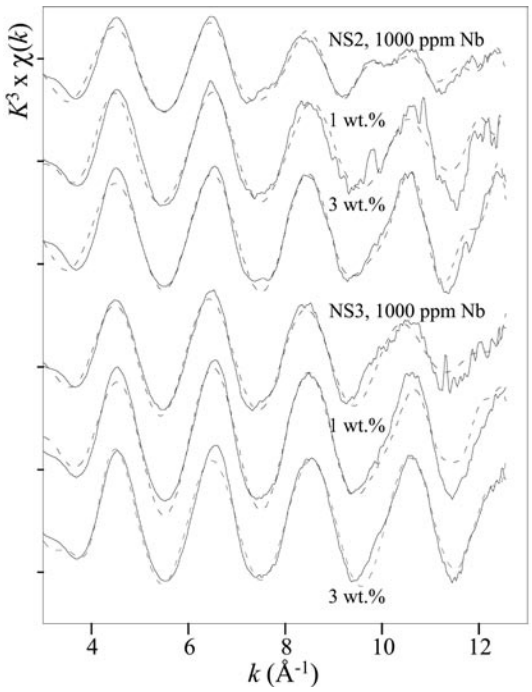

FIG. 7A. Nb *K*-edge normalized (k^3-weighted) EXAFS spectra for the NS2 and NS3 glasses (solid lines) and the best model (dashed lines) calculated on the basis of pyrochlore (two-shell fit).

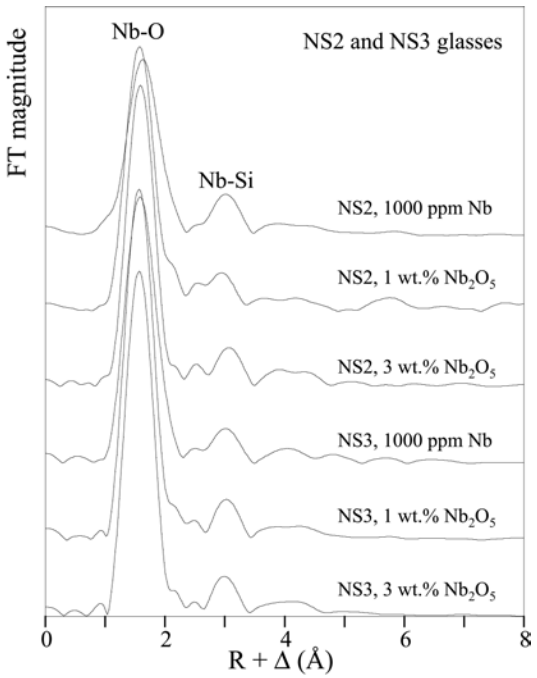

FIG. 7B. Fourier transforms of the normalized (k^3-weighted) EXAFS spectra for the ASI glasses.

Nb–Si contribution arising from four and seven second-nearest neighbors between 3.47 and 3.63 Å. The Nb–O bond lengths for the ASI 0.6 glasses range from 1.97 to 2.05 Å. However, in the "wet" ASI 1.2 glass with 1000 ppm Nb, the average Nb–O distance is much lower (1.88 Å), as shown also on the FTs (Fig. 8B) by a shift on the main Nb–O peak toward lower distances. Such Nb–O distances are typical of 6-coordinated Nb, in agreement with their XANES shape and low pre-edge feature. The ASI 0.6 "wet" glass with 1000 ppm Nb also shows a low distance-contribution on its FT (Fig. 8B). However, this contribution is weak and forms a shoulder on the FT near 1.2 Å. On the basis of the ionic radii of Nb (Shannon & Prewitt 1969), this shoulder would seem to be related to the presence of 5-coordinated environments around Nb in these two particular glasses. However, this information is inconsistent with the pre-edge feature and XANES edge-crest, which indicate the presence of 6-coordinated moieties around Nb. Therefore, we conclude that anharmonicity is severe around 6-coordinated Nb in the "wet" ASI 1.2 glass with 1000 ppm Nb. Anharmonicity is known to artificially decrease the average Nb–O distance where it is neglected in the models. In the present study, we considered the third cumulant (see the C^3 parameter in Tables 3 and 4) during the model to take into account the anharmonicity, but the C^3 parameters consider only relatively weak cases of anharmonicity. With the lack of simulations by molecular dynamics, it is difficult at this stage to determine the correct model for anharmonicity to include for this glass. We therefore consider this distance an artifact.

A second contribution is observed in both the ASI 0.6 and 1.2 glasses. The Nb–Si(Al) bond length for the peraluminous (ASI 1.2) glass is 3.61 Å (seven second neighbors), whereas the average <Nb–Si(Al)> bond length in the peralkaline (ASI 0.6) glasses is significantly shorter (3.49 Å), and the number of nearest neighbors decreases from seven in ASI 1.2 to between 4.2 and 6.6 in ASI 0.6. The increase in Nb–Si(Al) bond length and the number of second-nearest neighbors in the ASI 1.2 glass are consistent with increasing polymerization in the peraluminous glass.

Structural Role of Nb in Silicate Melts and Geochemical Implications

Results from the present study indicate that within the range of Nb_2O_5 contents studied (0.1 to 5.0 wt.%), Nb in dry, H_2O-saturated and F-bearing peraluminous and peralkaline glasses is 6-coordinated and resides in local environments that resemble those in natural Nb oxides and silicates. Niobium forms NbO_6 octahedra

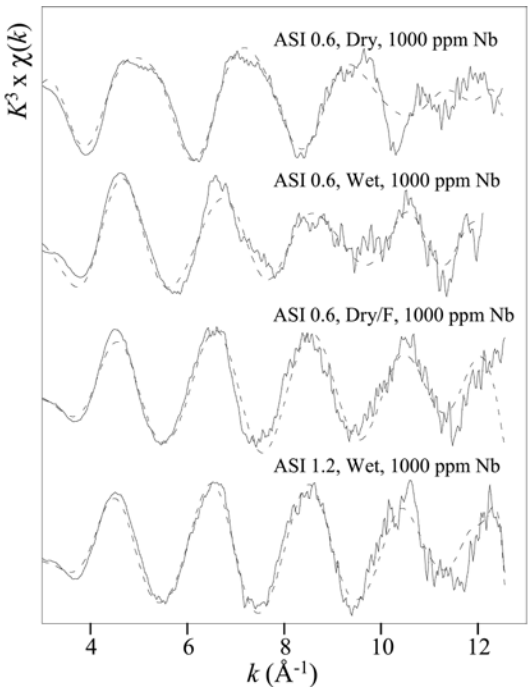

FIG. 8A. Nb *K*-edge normalized (k^3-weighted) EXAFS spectra for the ASI glasses (solid lines) and the best model (dashed lines) calculated on the basis of pyrochlore (two-shell fit).

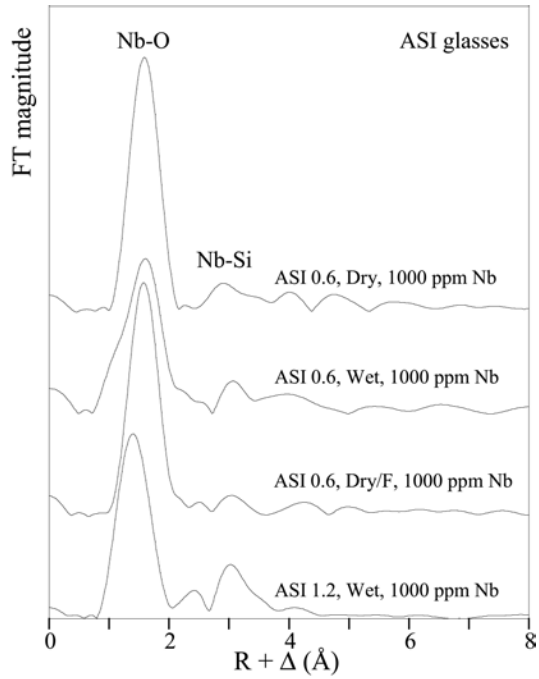

FIG. 8B. Fourier transforms of the normalized (k^3-weighted) EXAFS spectra for the ASI glasses.

(<Nb–O> = 2.04, 1.88 and 2.01 Å for NS, ASI 1.2 and ASI 0.6 glasses, respectively) that share corners with SiO_4 or AlO_4 tetrahedra (<Nb–Si> = 3.62, 3.61 and 3.49 Å for NS, ASI 1.2 and ASI 0.6, respectively). No evidence for 5-coordinated Nb was observed. The data are consistent with results from Raman scattering studies of M^{5+} cations in potassium silicate glasses by Ellison & Hess (1989) and with previous XAFS experiments (Gao *et al.* 1989, Cardinal *et al.* 1997).

Bond-length – bond-strength models for Nb

Plausible structural models for Nb^{5+} in silicate glasses can be constructed using Pauling's second rule for bond-valence requirements (Pauling 1929). Simple bond-valence analysis suggests that Nb^{5+} in 6-fold coordination will form bonds with O with bond strengths of 5/6 = 0.83 of a valence unit (*vu*). Bond lengths in NbO_6 octahedra range from 1.7 to 2.4 Å, (1.76 to 0.27 *vu*), with the mean in minerals being closer to 1.8 to 2.2 Å (1.35 to 0.46 *vu*). Individual Si–O bond lengths in silicate structures may vary between 1.54 and 1.70 Å (1.04 and 0.63 *vu*, respectively) and $^{[4]}$Al–O bond lengths range from 1.63 to 1.83 Å (1.06 to 0.63 *vu*, respectively). Similarly, Na–O bond lengths may vary from 2.2 to 3.4 Å, with bond strengths between 0.29 and <0.02 *vu*. If we fix the $^{[6]}$Nb–O bond length at the average length derived from the EXAFS spectra (1.98 Å, 0.83 *vu*), we can predict the local coordination environment around Nb in the silicate glasses (Fig. 9). Figure 9A shows that 6-coordinated Nb^{5+} cannot bond directly to either bridging oxygen atoms (BO) or to Si–O–Si linkages for bond-valence reasons: the BO is overbonded by 0.83 *vu*. To achieve a stable bond-valence configuration, the Nb–O and Si–O bond lengths would have to be stretched to their maximum values of 2.2 and 1.77 Å, respectively, resulting in extensive distortion and disruption of the glass network.

It is possible that Nb in the melt or glass bonds, in part, to $^{[4]}$Al–O–$^{[4]}$Al or Si–O–$^{[4]}$Al linkages as Nb–O–(Si,Al) species in peraluminous melts, or alternatively as Nb–O–(Na,K) species in peralkaline melts, as suggested by Horng *et al.* (1999). Substitution of Al for Si, along with a general weakening of the BO bonds of the network, would replace the need for charge compensation of the pentavalent Nb by alkali or alkaline earth cations. Using the Q^n notation (where *n* represents the average number of BO per tetrahedrally coordinated Si or Al cation), a concept first utilized in NMR studies of glass structure, we can describe the degree of polymerization of the network of tetrahedra in a melt. In general, with increasing Al_2O_3 in the melt, Al^{3+} exhibits a preference for Q^4 sites (*i.e.*, four BO; 70% of Al_{tot}), whereas Si is distributed amongst Q^2, Q^3 and Q^4 units (Mysen 2002, Mysen *et al.* 2003). In addition, ^{17}O NMR studies on Ca-aluminosilicate glasses suggest that NBOs show a strong preference to be localized on Si (Allwardt *et al.* 2003). This distribution depends primarily on the Al/(Al + Si) value. In the ASI 0.6 and 1.2 glasses, the ratio Al/(Al + Si) is almost identical (0.115 and 0.157, respectively), thus we expect a similar distribution of Q^4 *versus* Q^2 and Q^3 units, with Q^4 the dominant Al unit in both glass series. If Nb^{5+} forms Nb–O–Al complexes, we must first understand the variation in Al geometry and coordination in the glasses.

Toplis *et al.* (1997) suggested that the presence of triclusters, in which three Si or Al tetrahedra share a common BO ($AlSi_2O_{5.5}$ or $Al_2SiO_{5.5}$), and the apparent absence of NBOs in peraluminous melts, may be the key to understanding the solubility minima of elements such as Sn, Nb and Ta in granitic systems. However, there is no direct experimental evidence (NMR, XANES, *etc.*) for such triclusters, though they are present in molecular dynamic simulations (Benoit *et al.* 2001, Cormier *et al.* 2003), and Toplis *et al.* (1997) do not take into consideration alkaline compositions. Recently, some investigators have challenged the notion that Si and Al in tectosilicate glasses are fully polymerized (*i.e.*, do not have NBOs) and have indicated that four-membered rings of Al of tetrahedra are present in Al-rich glasses. Neuville *et al.* (2004) examined Ca-bearing tectosilicate and peraluminous glasses to determine the coordination of Al, in particular to quantify the proportion of $^{[5]}$Al in the glass and to help in understanding the presence of NBOs in such melts. They concluded that along with $^{[4]}$Al, there is a significant amount of $^{[5]}$Al in the glasses (7% and 28% in the tectosilicate and peraluminous glasses, respectively). The presence of such high proportions of $^{[5]}$Al in these glasses nullifies the need for the presence of triclusters in the melt or glass, in particular in peraluminous compositions, to explain the existence of additional NBOs. In addition, the presence of $^{[5]}$Al allows for the existence of Nb–O–$^{[5]}$Al linkages in the melt without the problem of overbonding of the network BOs or the need for an excess of alkalis.

However, it is more likely that Nb forms Nb–O–[(Al,Si)–(Na,K)] linkages through NBOs (Fig. 9B), particularly in the depolymerized peralkaline and H_2O- or F-bearing glasses. In such a case, the bond-valence sum of the NBO is satisfied with 0.83 *vu* from Nb, 1.0 *vu* from Si, with an additional 0.1 *vu* provided by additional alkali as a distant neighbor (*e.g.*, Na, Ca). Pauling's third rule suggests that polyhedra about Nb and network modifiers such as Na must share edges, with Nb–O–Na angles close to 100°. Niobium therefore acts as a network modifier in both peraluminous and peralkaline silicate glasses, similar to Zr and Sn (Farges *et al.*, *in press*). Linkages of Nb–O–Nb also are possible, but the presence of such second neighbors could not be unequivocally proven in this study.

Geochemical implications

The extrapolation of the speciation information for transition elements in silicate glasses to natural high-pressure and high-temperature melts of geochemical

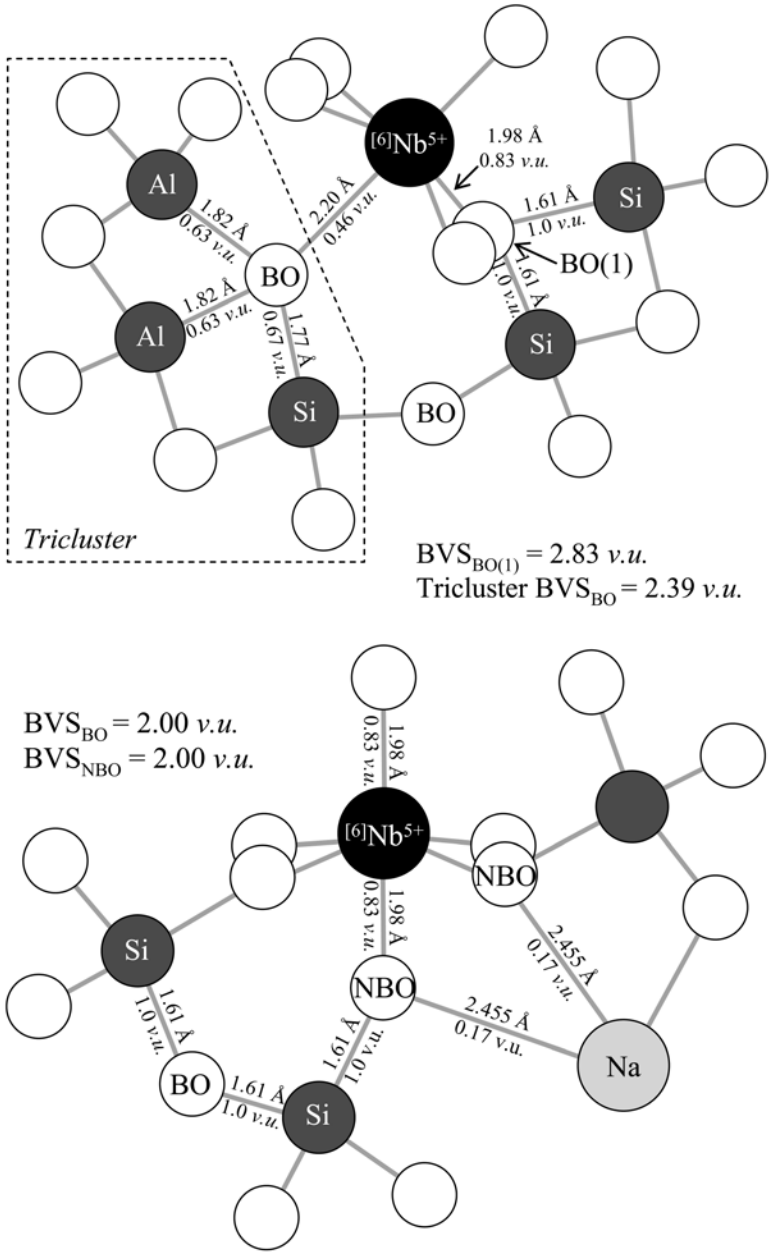

FIG. 9. Bond-length – bond-strength models for NbO_6 octahedra in the silicate glasses. A. Unlikely model: NbO_6 as a network former and linked to a tricluster. Note that the bridging atoms of oxygen (BO) are overbonded. B. Probable model: NbO_6 as a network modifier with additional network-modifying alkali cations (Na). Both the bridging (BO) and non-bridging atoms of oxygen (NBO) have their average bond-valence requirements satisfied.

interest is always delicate (see Brown *et al.* 1995 for a review). In the case of Nb^{5+}, its relatively high average bond-valence (0.83 *vu*) makes this pentavalent cation only weakly sensitive to polyhedron compressibility or thermal expansion, as bond valence is directly related to the average coefficient of linear thermal expansion ($\bar{\alpha}$, Farges & Brown 1996). For 6-coordinated Nb^{5+}–O bonds, $\bar{\alpha}$ is calculated to be $\sim 4.5 \times 10^{-6}$ K^{-1}, suggesting a thermal expansion of less than 0.01 Å at 1500°C. On the other hand, the naturally occurring and chemically complex glasses [see Fig. 5; structural and chemical details for these particular glasses can be found in Farges & Rossano (2000)] all show fairly similar Nb *K*-edge XANES spectra as for the synthetic, chemically simpler glasses. Therefore, the information obtained here for synthetic and natural glasses is likely to be transferable to *in situ* complex melts, as already demonstrated for Zr^{4+} to 1450°C and 50 kbar (Muñoz & Farges, unpubl. rep.).

Variations in the local environment of Nb in the synthetic glasses related to the degree of polymerization of the melt have also been documented. Depolymerization of a silicate melt can be accomplished by a number of factors (Mysen 1988, Dingwell *et al.* 1996): (1) addition of alkali elements to decrease the ASI index of the glasses, effectively increasing the proportion of NBOs to which Nb may bond, (2) addition of H_2O (except in Al-bearing and fully polymerized compositions; see McMillan 1994, Kohn 2000, Schmidt *et al.* 2001, Behrens & Nowak 2003), and (3) addition of F (see Kohn *et al.* 1990, 1991, Schaller *et al.* 1992, Kiczenski *et al.* 2004). We found that all three factors have had an influence on the glasses studied here. The effects of depolymerization by addition of network-modifying alkali cations can be observed in the variations in the Nb *K*-edge XANES spectra of the ASI 0.6 and ASI 1.2 glasses, as well as in the coordination environment of the second-nearest neighbors around Nb, as shown in the EXAFS spectra. In the XANES spectra, we observed that Nb is sensitive to the lack of NBOs in the peraluminous compositions (ASI 1.2) such that as peraluminosity increases (the number of NBO decreases), the distortion of the NbO_6, along with the local disorder, increases. In addition, an increase in the <Nb–Si(Al)> distance and number of second-nearest neighbors is observed in the ASI 1.2 glass, a result of increasing polymerization and decreasing network-modifying alkali elements within the peraluminous compositions. Peraluminous glasses contain NbO_6 environments more similar to those of the manganocolumbite than the alkali niobosilicate minerals; H_2O- or F-bearing peralkaline glasses have local environments that are less distorted and more ordered, resembling those in alkali niobosilicate minerals such as vuonnemite.

It has long been known that the addition of H_2O and F has a profound affect on the physical and chemical properties of a melt (Giordano *et al.* 2004). In granitic systems, H_2O lowers the melt viscosity by several orders of magnitude (*e.g.,* Shaw 1963, Dingwell *et al.* 1996, Whittington *et al.* 2000); H_2O and volatiles such as F, CO_3 and P act as fluxes, lowering the eutectic, solidus and liquidus temperatures (*e.g.,* Tuttle & Bowen 1958). In addition, they control the phase equilibria (*e.g.,* Whitney 1975), increase the rate of crystal settling and bubble ascent (Dingwell *et al.* 1985), and dramatically increase the solubility of Nb owing to the stability of Nb–F and Nb–CO_3 within carbonate-, fluoride- and phosphate-rich fluids at temperatures between 50 and 450°C (Aleksandrov 1967, Möller 1986, Keppler 1993). In addition, H_2O and F depolymerize the melt structure by liberating NBOs ($H_2O + O^{2-} = 2OH^-$ and $F_2O^- + O^{2-} = 2F^- + 2O^{2-}$) to which Nb can bond, thus increasing its solubility, a feature that is particularly evident in granitic systems (Keppler 1993, Kohn 2000, Kiczenski *et al.* 2004). In the absence of H_2O, F forms complexes with Al (AlF_6^{3-} or AlF_5^{2-}), liberating alkalis from their charge-balancing role and depolymerizing the melt or glass. In the presence of H_2O, F preferentially reacts with the silicate network, substituting for a BO, and creating non-bridging F rather than forming complexes with Al (Giordano *et al.* 2004). In both cases, the proportion of NBOs to which Nb can bond is increased.

Within the ASI glasses, NbO_6 octahedra share corners *via* NBOs with network-forming Si and Al tetrahedra; alkalis such as Na and K act as charge-balancing cations. In general, although the ratio Al/(Al + Si) is essentially identical in both sets of glasses, the ASI 1.2 series contain a higher proportion of network-modifying $^{[6]}$Al than the peralkaline glasses, which contain a greater proportion of alkalis and $^{[4]}$Al (Dingwell *et al.* 1985). The depolymerizing effects of H_2O and F are more evident within the peraluminous compositions, in which NBO are lacking in dry compositions; an increase in the H_2O and F contents results in a less-ordered, non-centrosymmetric local environment around Nb. Release of NBOs from the network and formation of Nb–O–Al (*i.e.,* not bonded to Si) and Al–F complexes decrease the local order of the central Nb cation. Ideally, this should also be the case in the peralkaline glasses. However, we observe a reverse trend in the ASI 0.6 glasses with 1000 ppm Nb: with increasing H_2O and F content, the NbO_6 octahedra become more ordered and centrosymmetric. As stated earlier, a number of factors could be the cause of this reverse trend, and further studies on the local structure of the melt in terms of Si, Al and Na are required before an exact cause is outlined. We contend that the above variation in F and Al complexing within the two melt compositions is directly responsible, and the addition of F and H_2O to an alkali-rich peralkaline melt results in the formation of Nb–O–[(Si,Al)–Na] complexes, where Nb proxies for either tetrahedrally coordinated Si or Al lost in the formation of SiF_6^{2-} or AlF_6^{3-} complexes, as suggested by Giordano *et al.* (2004).

In granites and syenites, the average Nb content ranges from 0.002 to 0.031 wt.% Nb_2O_5, with Nb dispersed in rock-forming silicates (micas, pyroxenes and amphiboles) and in oxides (columbite, perovskite and pyrochlore along with magnetite, ilmenite, rutile, titanite and zircon; Vlasov 1996). Enrichments and economic deposits of Nb (up to 15 wt.% Nb_2O_5) are generally associated with postmagmatic or hydrothermal veins, greisen zones, fractures and pegmatites within granites, alkali granites (Pollard 1989a), nepheline syenites, fenites, and carbonatites related to alkali ultramafic complexes (Vlasov 1996). These observations in nature are in agreement with the above speciation and solubility information obtained experimentally. Pollard (1989b) also observed that enrichment in Nb can either be the consequence of enrichment in the apical region of a zoned magmatic chamber by fractionation, or by migration of postmagmatic fluids, which leach Nb from the base of the chamber and concentrate it at the top. Rarely are economic concentrations of Nb formed during early, magmatic stages of crystallization; they are generally associated with late-stage, postmagmatic processes (Vlasov 1996). Consequently, the role of postmagmatic fluids and the transport of Nb under hydrothermal conditions must be investigated in more detail in light of the information obtained here for H_2O- and F-bearing glasses.

Conclusions

In dry, H_2O and F-bearing peraluminous and peralkaline glasses containing between 0.1 and 5 wt.% Nb_2O_5, Nb^{5+} is present as NbO_6 moeties that share corners with SiO_4 and AlO_4 tetrahedra through non-bridging atoms of oxygen. No evidence for 4-, 5- or 7-coordinated Nb was found. Bond-valence requirements are fulfilled by the presence of network-modifying alkali cations such as Na and K. This environment most closely resembles those observed in alkali niobosilicates such as vuonnemite and labuntsovite-group minerals. In dry, peraluminous glasses, the sites containing Nb are non-centrosymmetric and disordered, similar to what is observed for oxide minerals such as columbite. Increasing order and centrosymmetry are noted in peralkaline, sodium disilicate and trisilicate glasses. Addition of H_2O and F to peraluminous compositions results in decreased order and increased distortion of the NbO_6 environment. In peralkaline compositions, the addition of H_2O and F has a reverse effect, increasing the degree of order and decreasing the distortion of the NbO_6 environment. The local environment around the Nb atoms is highly sensitive to melt depolymerization, alkalinity, H_2O and F contents, all of which will increase the solubility of Nb in the melt.

Acknowledgments

The authors thank the following people for their help and support during the course of this project: V. Malavergne, M. Munoz & S. Rossano (Univ. de Marne-la-Vallée), B. Reynard (ENS, Lyon), T.S. Ercit (CMN), and A.M. McDonald (Laurentian). Funding for this project was provided by NSERC in the form of a post-doctoral fellowship to PCP, the Canadian Museum of Nature in the form of a RAC operating grant to PCP, Bayerisches Geoinstitut (RLL), NSERC (RLL), and SSRL. The Stanford Synchrotron Radiation Laboratory is supported by DOE, Office of Basic Energy Sciences, and NIH, Biotechnology Resource Program, Division of Research Resources. Constructive, detailed comments by two referees, L. Cormier and A. Anderson, as well as Associate Editor I.M. Samson, are greatly appreciated.

References

Aleksandrov, I.V. (1967): Niobium in carbon dioxide solutions and considerations concerning migration of rare elements under hydrothermal conditions. *Geokhimiya*, 684-693. (Engl. Version available?)

Allwardt, J.R., Lee, S.K. & Stebbins, J.F. (2003): Bonding preferences of non-bridging O atoms: evidence from ^{17}O MAS and 3QMAS NMR on calcium aluminate and low-silica Ca-aluminosilicate glasses. *Am. Mineral.* **88**, 949-954.

Behrens, H. & Nowak, M. (2003): Quantification of water speciation in silicate glasses and melts by IR spectroscopy – in situ vs. quench technique. *Phase Trans.* **76**, 45-61

Benoit, M., Ispas, S. & Tuckerman, M.E. (2001): Structural properties of molten silicates from ab initio molecular-dynamics simulations: comparison between $CaO–Al_2O_3–SiO_2$ and SiO_2. *Phys. Rev. B*, **64**, 224205-1 - 224205-10.

Bianconi, A., Fritsch, E., Calas, G. & Petiau, J. (1985): X-ray absorption near edge structure of 3d transition elements in tetrahedral coordination. The effect of bond length variation. *Phys. Rev. B* **32**, 4292-4295.

de Bournonville, M.B., Bizot, D. Chassaing, J. & Quarton, M. (1986): Structures et propriétés magnétiques de Li_2NbF_6 et Na_2NbF_6. *J. Solid State Chem.* **62**, 212-219.

Brown, G.E., Jr., Farges, F. & Calas, G. (1995): X-ray scattering and X-ray spectroscopy studies of silicate melts. *In* Structure, Dynamics and Properties of Silicate Melts (J.F. Stebbins, P.F. McMillan & D.B. Dingwell, eds.). *Rev. Mineral.* **32**, 317-410.

Brown, G.M. & Walker, L.A. (1966): Refinement of the structure of potassium heptafluoroniobate, K_2NbF_7, from neutron-diffraction data. *Acta Crystallogr.* **20**, 220-229.

CARDINAL, T., FARGIN, E., LE FLEM, G., COUZI, M., CANIONI, L., SEGONDS, P., SARGER, L., DUCASSE, A. & ADAMIETZ, F. (1996): Nonlinear optical properties of some niobium (V) oxide glasses. *Eur. J. Sol. State Inorg. Chem.* **33**, 597-605.

CARDINAL, T., FARGIN, E., LE FLEM, G. & LEBOITEUX, S. (1997): Correlations between structural properties of Nb_2O_5–$NaPO_3$–$Na_2B_4O_7$ glasses and non-linear optical activities. *J. Non-Cryst. Solids* **222**, 228-234.

ČERNÝ, P. & ERCIT, T.S. (1989): Mineralogy of niobium and tantalum: crystal chemical relationships, paragenetic aspects and their economic applications. *In* Lanthanides, Tantalum and Niobium (P. Möller, P. Černý & F. Saupé, eds.). Springer Verlag, Berlin, Germany (27-79).

CHUKANOV, N.V., PEKOV, I.V., RASTSVETAEVA, R.K. & NEKRASOV, A.N. (1999): Labuntsovite: solid solutions and features of the crystal structure. *Can. Mineral.* **37**, 901-910.

COHEN, R.E. (1992): Origin of ferroelectricity in perovskite oxides. *Nature* **358**, 136-139.

CORMIER, L., GHALEB, D., NEUVILLE, D.R., DELAYE, J.-M. & CALAS, G. (2003): Chemical dependence of network topology of calcium aluminosilicate glasses: a molecular dynamics and reverse Monte Carlo study. *J. Non-Cryst. Solids* **332**, 255-270.

DINGWELL, D.B., ROMANO, C. & HESS, K.-U. (1996): The effect of water on the viscosity of a haplogranitic melt under P–T–X conditions relevant to silicic volcanism. *Contrib. Mineral. Petrol.* **124**, 19-28.

DINGWELL, D.B., SCARFE, C.M. & CRONIN, D.J. (1985): The effect of fluorine on viscosities in the system Na_2O–Al_2O_3–SiO_2: implications for phonolites, trachytes and rhyolites. *Am. Mineral.* **70**, 80-87.

DUNN, T. & MCCALLUM, I.S. (1982): The partitioning of Zr and Nb between diopside and melts in the system diopside–albite–anorthite. *Geochim. Cosmochim. Acta* **46**, 623-629.

EDWARDS, A.J. (1964): The structures of niobium and tantalum pentafluorides. *J. Chem. Soc.*, 3714-3718.

ELJAZOULI, A., VIALA, J.C., PARENT, C., LEFLEM, G. & HAGENMULLER, P. (1988): Structural investigation of glasses belonging to the Na_2O–Nb_2O_5–P_2O_5 system. *J. Sol. State Chem.* **73**, 433-439.

ELLISON, A.J. & HESS, P.C. (1989): Solution mechanisms of period V cations in potassium silicate glasses: inferences from Raman spectra. *Trans. Am. Geophys. Union* (*Eos*) **70**, 87 (abstr.).

ERCIT, T.S., COOPER, M.A. & HAWTHORNE, F.C. (1998): The crystal structure of vuonnemite, $Na_{11}Ti^{4+}Nb_2(Si_2O_7)_2(PO_4)_2O_3(F,OH)$, a phosphate-bearing sorosilicate of the lomonosovite group. *Can. Mineral.* **36**, 1311-1320.

FARGES, F. & BROWN, G.E., JR. (1996): An empirical model for the anharmonic analysis of high-temperature XAFS spectra of oxide compounds with applications to the coordination environment of Ni in Ni-olivine and Ni–Na-disilicate glass and melt. *Chem. Geol.* **127**, 253-268.

FARGES, F., LINNEN, R.L. & BROWN, G.E., JR. (2006): Redox and speciation of tin in hydrous silicate glasses: a comparison with nb, Ta, Mo and W. *Can. Mineral.* **44**, 795-810.

FARGES, F., PONADER, C.W. & BROWN, G.E., JR. (1991): Local environment around incompatible elements in silicate glass/melt systems. I. Zr at trace levels. *Geochim. Cosmochim. Acta* **55**, 1563-1574.

FARGES, F. & ROSSANO, S. (2000): Water in Zr-bearing synthetic and natural glasses. *Eur. J. Mineral.* **12**, 1093-1107.

FUKUMI, K. & SAKKA, S. (1988): Coordination state of Nb^{5+} ions in silicate and galate glasses as studied by Raman spectroscopy. *J. Mater. Sci.* **23**, 2819-2823.

FUKUMI, K. & SAKKA, S. (1989): Structure of alkali or alkaline earth niobium gallate glasses. *J. Non-Cryst. Solids* **110**, 61-68.

GAO, H.X., WANG, Z.C. & WANG, S.H. (1989): Properties and structure of niobosilicate glasses. *J. Non-Cryst. Solids* **112**, 332-335.

GIORDANO, D., ROMANO, C., DINGWELL, D.B., POE, B. & BEHRENS, H. (2004): The combined effects of water and fluorine on the viscosity of silicic magma. *Geochim. Cosmochim. Acta* **68**, 5159-5168.

HORNG, W.-S., HESS, P.C. & GAN, H. (1999): The interactions of M^{+5} cations (Nb^{+5}, Ta^{+5}, or P^{+5}) and anhydrous haplogranite melts. *Geochim. Cosmochim. Acta* **63**, 2419-2428.

KEPPLER, H. (1993) Influence of fluorine on the enrichment of high field strength trace elements in granitic rocks. *Contrib. Mineral. Petrol.* **114**, 479-488.

KICZENSKI, T.J., DU, L.-S. & STEBBINS, J.F. (2004): F–19 NMR study of ordering of high field strength cations at fluoride sites in silicate and aluminosilicate glasses. *J. Non-Cryst. Solids* (in press).

KLEMENTIEV, K.V. (2001): Viper for Windows. *J. Phys. D: Appl. Phys.* **34**, 209-217. Freeware available at http://www.desy.de/~klmn/viper.html. Or 1989???

KOHN, S.C. (2000): The dissolution mechanisms of water in silicate melts; a synthesis of recent data. *Mineral. Mag.* **64**, 389-408.

KOHN, S.C., CHARNOCK, J.M., HENDERSON, C.M.B. & GREAVES, G.N. (1990): The structural environments of trace elements in dry and hydrous silicate glasses. A manganese and strontium K-edge X-ray absorption spectroscopic study. *Contrib. Mineral. Petrol.* **105**, 359-368.

KOHN, S.C., DUPREE, R., MORTUZA, M.G. & HENDERSON, C.M.B. (1991): NMR evidence of five- and six-coordinated aluminum fluoride complexes in F-bearing aluminosilicate glasses. *Am. Mineral.* **76**, 309-312.

KOSTRUN, V.O., CEHN, M.H. & CRASEMANN, B. (1971): Atomic radiation transition probabilities to the 1s state and theoretical K-shell fluorescence yields. *Phys. Res. B* **3**, 533-545.

KUNZ, M. & BROWN, D. (1995): Out-of-center distortions around octahedrally-coordinated d^0 transition metals. *J. Solid State Chem.* **115**, 395-406.

LINNEN, R. & KEPPLER, H. (1997): Columbite solubility in granitic melts: consequences for the enrichment and fractionation of Nb and Ta in the Earth's crust. *Contrib. Mineral. Petrol.* **128**, 213-227.

MAHOOD, G. & STIMAC, J.A. (1990): Trace-element partitioning in pantellerites and trachytes. *Geochim. Cosmochim. Acta* **54**, 2257-2276.

MARKGRAF, S.A., HALLIYAL, A., BHALLA, A.S. & NEWNHAM, R.E. (1985): X-ray structure refinement and pyroelectric investigation of fresnoite, $Ba_2TiSi_2O_8$. *Ferroelectrics* **62**, 17-26.

MCMILLAN, P. F. (1994): Water solubility and speciation models. *In* Volatiles in Magmas (M.R. Carroll & J.R. Holloway, eds.). *Rev. Mineral.* **30**, 131-156.

MEGAW, H.D. (1968a): A simple theory of the off center displacement of cations in octahedral environments. *Acta Crystallogr.* **B24**, 149-153.

MEGAW, H.D. (1968b): The thermal expansion of interatomic bonds, illustrated by experimental evidence from certain niobates. *Acta Crystallogr.* **A24**, 589-604.

MÖLLER, P. (1986): REE(Y), Nb, and Ta enrichment in pegmatites and carbonatite-alkalic rock complexes. *In* Lanthanides, Tantalum and Niobium (P. Möller, P. Černý & F. Saupé, eds.). Springer-Verlag, Berlin, Germany (103-144).

MOORE, P.B., TAKAHARU, A., KAMPF, A.R. & STEELE, I.M. (1976): Olmsteadite, $K_2Fe^{2+}{}_2$ $[Fe^{2+}(Nb,Ta)_2O_4(H_2O)_4(PO_4)_4]$, a new species, its crystal structure and relation to vauxite and montgomeryite. *Am. Mineral.* **61**, 5-11.

MYSEN, B.O. (1988): *Structure and Properties of Silicate Melts*. Elsevier, Amsterdam, The Netherlands.

MYSEN, B.O. (2002): Physics and chemistry of silicate glasses and melts. *Eur. J. Mineral.* **15**, 781-802.

MYSEN, B.O., LUCIER, A. & CODY, G.D. (2003): The structural behavior of Al^{3+} in peralkaline melts and glasses in the system Na_2O–Al_2O_3–SiO_2. *Am. Mineral.* **88**, 1668-1678.

NEIVA, A.M.R. (1999): Niobium. *In* Encyclopedia of Geochemistry (C.P. Marshall & R.W. Fairbridge, eds.). Kluwer Academic Publishers, Dordrecht, The Netherlands.

NEUVILLE ET AL. (2004):

PARIS, E., GIULI, G., ROMANO, C., DINGWELL, D. & DAVOLI, I. (2000): Niobium, tantalum and tungsten in silicate glasses: structural and geochemical role by XAS. EMPG VIII (Bergamo, Italy). *Conf. Abstr.* **5**, 82.

PAULING, L. (1929): The principles determining the structure of complex ionic crystals. *J. Am. Chem. Soc.* **51**, 1010-1026.

PICHAVANT, M., HERRERA, J.V., BOULMIER, S., BRIQUEU, L., JORON, J.-L., JUTEAU, M., MARIN, L., MICHARD, A., SHEPPARD, S.M.F., TREUIL, M. & VERNET, M. (1987): The Macusani glasses, SE Peru: evidence of chemical fractionation in peraluminous magmas. *Geochem. Soc., Spec. Publ.* **1**, 359-373.

POLLARD, P.J. (1989a): Geochemistry of granites associated with tantalum and niobium mineralization. *In* Lanthanides, Tantalum and Niobium (P. Möller, P. Černý & F. Saupé, eds.). Springer Verlag, Berlin, Germany (145-170).

POLLARD, P.J. (1989b): Geologic characteristics and genetic problems associated with the development of granite-hosted deposits of tantalum and niobium. *In* Lanthanides, Tantalum and Niobium (P. Möller, P. Černý & F. Saupé). Springer Verlag, Berlin, Germany (240-256).

REHR, J.J., ZABINSKY, Z.I. & ALBERS, R.C. (1992): High-order multiple scattering calculations of x-ray absorption fine structure. *Phys. Rev. Lett.* **69**, 3397-4000.

SAMUNEVA, B., KRALCHEV, S. & DIMITROV, V. (1991): Structure and optical properties of niobium silicate glasses. *J. Non-Cryst. Solids* **129**, 54-63.

SANTOS, C.A. DOS, ZAWISLAK, L.I., KINAST, E.J., ANTOIETTI, V. & DA CUNHA, J.B.M. (2001): Crystal chemistry and structure of the orthorhombic $(Fe,Mn)(Ta,Nb)_2O_6$ family of compounds. *Braz. J. Phys.* **31**, 616-631.

SCHALLER, T., DINGWELL, D.B., KEPPLER, H., KNÖLLER, W., MERWIN, L. & SEBALD, A. (1992): Fluorine in silicate glasses: a multinuclear nuclear magnetic resonance study. *Geochim. Cosmochim. Acta* **56**, 701-707.

SCHMIDT, B.C., RIEMER, T., KOHN, S.C., HOLTZ, F. & DUPREE, R. (2001): Structural implications of water dissolution in haplogranitic glasses from NMR spectroscopy: influence of total water content and mixed alkali effect. *Geochim. Cosmochim. Acta* **65**, 2949-2964.

SHANNON, R.D. & PREWITT, C.T. (1969): Effective ionic radii in oxides and fluorides. *Acta Crystallogr.* **B25**, 925-945.

SHAW, H.R. (1963): Obsidian–H_2O viscosities at 1000 and 2000 bars in the temperature range 700° to 900°C. *J. Geophys. Res.* **68**, 6337-6343.

TOPLIS, M.J., DINGWELL, D.B. & LENCI, T. (1997): Peraluminous viscosity maxima in Na_2O–Al_2O_3–SiO_2 liquids: the role of triclusters in tectosilicate melts. *Geochim. Cosmochim. Acta* **61**, 2605-2612.

TUTTLE, O.F. & BOWEN, N.L. (1958): Origin of granite in light of experimental studies in the system $NaAlSi_3O_8$–$KAlSi_3O_8$–SiO_2–H_2O. *Geol. Soc. Am., Mem.* **74**.

VLASOV, K.A. (1996): Niobium. *In* Geochemistry and Mineralogy of Rare Elements and Genetic Types of their Deposits **1** (K.A. Vlasov, ed.). Israel Scientific Tranlations, Jerusalem, Israel (335- 367).

VOGEL, E.M., KOSINSKI, S.G., KROL, D.M., JACKEL, J.L., FRIBERG, S.R., OLIVER, M.K. & POWERS, J.D. (1989): Structural and optical study of silicate glasses for nonlinear optical devices. *J. Non-Cryst. Solids* **107**, 244-250.

WHITNEY, J.A. (1975): The effects of pressure, temperature and XH_2O on phase assemblage in four synthetic compositions. *J. Geol.* **83**, 1-31.

WHITTINGTON, A., RICHET, P. & HOLTZ, F. (2000): Water and the viscosity of depolymerised aluminosilicate melts. *Geochim. Cosmochim. Acta* **64**, 3725-3736.

WINTERER, M. (1996): The XAFS package. *In* IX Int. Conf. on X-ray Absorption Fine Structure (J. Goulon, C. Goulon-Ginet & N.B. Brookes, eds.). Les Editions de Physique, Les Ulis, France (Publ. **144**).

Received January 16, 2005, revised manuscript accepted September 30, 2005.